JOURNAL OF GEOPHYSICAL RESEARCH, VOL. 106, NO. C5, PAGES 9603–9621, MAY 15, 2001

Lateral dispersion over the continental shelf: Analysis of dye release experiments

Miles A. Sundermeyer[1]

Joint Program in Physical Oceanography, Massachusetts Institute of Technology/Woods Hole Oceanographic Institution, Woods Hole, Massachusetts

James R. Ledwell

Department of Applied Physics and Ocean Engineering, Woods Hole Oceanographic Institution, Woods Hole, Massachusetts

Abstract. Lateral dispersion over the continental shelf was examined using dye studies performed as a part of the Coastal Mixing and Optics experiment. Four experiments performed at intermediate depths, each lasting 2.5–5 days, were examined. In some cases the dye patches remained fairly homogeneous both vertically and horizontally throughout an experiment. In other cases, significant patchiness was observed on scales ranging from 2 to 10 m vertically and a few hundred meters to a few kilometers horizontally. The observations showed that the dye distributions were significantly influenced by shearing and straining on scales of 5–10 m in the vertical and 1–10 km in the horizontal. Superimposed on these larger-scale distortions were simultaneous increases in the horizontal second moments of the dye patches, with corresponding horizontal diffusivities based on a Fickian diffusion model of 0.3–4.9 $m^2\ s^{-1}$. Analysis of the dye data in concert with shear estimates from shipboard acoustic Doppler current profiler observations showed that the existing paradigms of shear dispersion and dispersion by interleaving water masses cannot account for the observed diffusive spreading of the dye patches. This result suggests that some other mechanisms provided an additional diffusivity of order 0.2–4.6 $m^2\ s^{-1}$. An alternative mechanism, dispersion by vortical motions caused by the relaxation of diapycnal mixing events, may explain the observed dispersion in some cases.

1. Introduction

It has long been known that lateral dispersion in the ocean is not solely the result of molecular processes but rather is significantly enhanced by shearing and straining on scales ranging from millimeters to hundreds of kilometers. As described by *Richardson* [1926] and *Richardson and Stommel* [1948], the effective horizontal diffusivity observed in both the atmosphere and the ocean depends on the scale of the phenomenon in question. This result was concisely summarized in a diffusion diagram by *Stommel* [1949] that showed that the effective horizontal diffusivity κ_H on scales ranging from $l = 0.2$ to 100 m varied approximately as $\kappa_H \propto l^{\frac{4}{3}}$ (*Richardson* [1926] also showed a similar diagram for his atmospheric observations). This $\frac{4}{3}$ power law was predicted by the similarity theories of turbulence of *Kolmogorov* [1941] and *Batchelor* [1950]. More recently, a collection of empirical data from dye experiments in the surface mixed layer was compiled by *Okubo* [1971]. These experiments, ranging in scale from 100 m to 100 km, also showed that the effective diffusivity increased as a function of horizontal scale, in this case $\kappa_H \propto l^{1.1}$. (As suggested by Okubo, his findings do not rule out the possibility that the $\frac{4}{3}$ power law of diffusivity could be valid locally for some time and length scales.)

The diffusion diagrams of *Okubo* [1971] have been used by many investigators as benchmarks for comparing experimental results from a wide range of space scales and timescales. Such diagrams provide not only a clue to the behavior of oceanic dispersion but also a practical means of comparing and predicting the dispersion at different scales. However, as suggested by *Okubo* [1971, p. 799], "any interpretation of the diffusion diagrams must remain provisional until the mechanisms or physical processes giving rise to diffusion are well understood."

Numerous tracer release studies have been performed by previous investigators both in coastal environments

[1]Now at School of Marine Science and Technology, University of Massachusetts Dartmouth, New Bedford.

Paper number 2000JC900138.
0148-0227/01/2000900138 $09.00

and in freshwater lakes in an effort to explain the mechanisms and physical processes that control horizontal dispersion in the ocean. However, very few of these have been in stratified environments. Noteworthy exceptions include experiments in the Baltic Sea by *Kullenberg* [1971], experiments off the east coast of Florida by *Vasholz and Crawford* [1985], a recent Florida Shelf Lagrangian Experiment by *Wanninkhof et al.* [1997], bottom boundary layer experiments off the New England shelf by *Houghton* [1997], the Massachusetts Bay dye studies by *Geyer and Ledwell* [1994, 1997], and the Coastal Mixing and Optics (CMO) dye experiments discussed in the present work. These experiments provide an invaluable opportunity to evaluate a wide range of dispersion models in the presence of stratification.

In the present study, tracer-release studies from CMO are used to examine the rates and mechanisms of lateral dispersion in the coastal ocean. Dispersion on scales of a few hundred meters to 10 km and for periods ranging from 2.5 to 5 days is examined. It is shown that the existing paradigms of lateral dispersion by vertical shear dispersion, lateral intrusions of differing water masses, and diffusive interleaving cannot explain the dispersion observed during the dye experiments. An alternative mechanism, dispersion by vortical motions caused by the relaxation of diapycnal mixing events, is suggested and briefly discussed.

1.1. Reversible and Irreversible Processes

There are many ways to quantify dispersion in the ocean, depending on the problem of interest. One way that is useful for the purposes of the present study is to classify dispersion as either "reversible" or "irreversible." By reversible dispersion we mean spreading of tracer by purely advective processes, for example, some arrangement of vertical and horizontal shears or strains that displaces the dye without diffusing it. Such processes are reversible in the sense that they do not alter the concentration of tracer following fluid parcels. Hence, in principle, it is always possible for the advection to reverse direction and restore the tracer to its initial distribution. (Note, this means that the reversible dispersion may be negative at times.) In contrast, irreversible dispersion does change the tracer concentration of individual fluid parcels and cannot be reversed. Molecular diffusion is the most elementary irreversible dispersion process. However, in practice, irreversible dispersion may also include stirring by small-scale shears and strains, as well as diffusive processes that were not resolved in the observations (i.e., some stirring plus molecular diffusion will insure irreversibility before any real reversal occurs).

With this distinction between reversible and irreversible dispersion in mind we define two measures of lateral dispersion during the CMO dye experiments. The first is the effective horizontal diffusivity κ_ζ estimated from the vertically integrated tracer (Figure 1a). This gives a measure of the overall (total) horizontal spreading of the dye patch and can be thought of as a sum of reversible and irreversible processes in the sense that it includes both the advective effects of vertical shears and the effective diffusion due to small-scale mixing and stirring processes. This total dispersion is relevant in problems where the lateral but not the vertical extent of the tracer is of interest. It is also useful for comparison with mixed layer studies in which global horizontal variances are identical to the depth-dependent variances, and with historical dye studies where the vertical integral of tracer was the only observed quantity.

The second measure of lateral dispersion is the effective irreversible horizontal diffusivity κ_{irrev} estimated

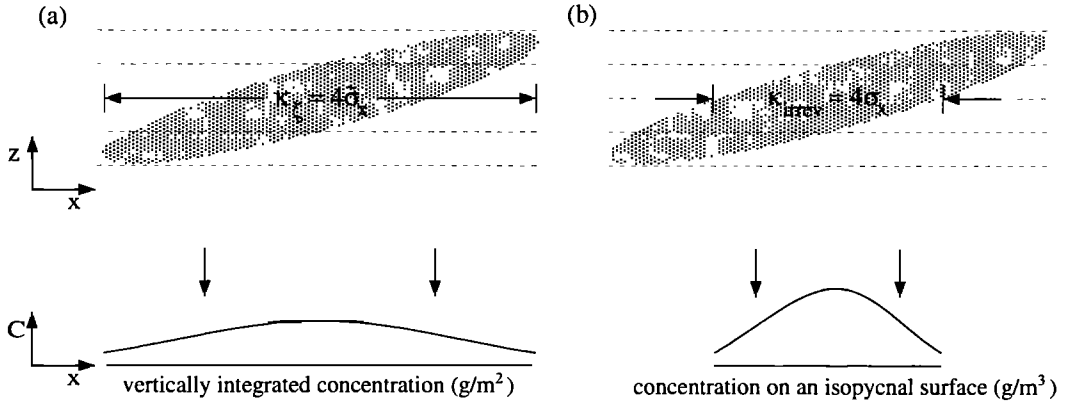

Figure 1. Schematic showing the distinction between (a) total dispersion (reversible plus irreversible) and (b) irreversible dispersion. The shaded regions in each panel represent a section through a hypothetical dye patch some finite time after a point source release. The vertical tilt of the dye patch is presumed to be due to vertical shear. The total dispersion, represented in Figure 1(a), is a measure of the vertical tilt of the patch as well as the spreading of tracer along isopycnals. Irreversible dispersion, represented in Figure 1(b), is a measure only of the spreading along a single isopycnal.

from the dye concentration along an isopycnal surface (Figure 1b). This diffusivity takes into account the depth dependence of the tracer. For example, κ_{irrev} does not directly include the advective effects of vertical shears since these represent relative motions of isopycnals. However, it does include horizontal diffusion due to vertical shear dispersion, i.e., the interaction between vertical shear and vertical diffusion, since this involves spreading of dye along isopycnals. The advective effects of larger-scale horizontal strains are also not included as part of κ_{irrev}, but rather will be treated explicitly in the forthcoming analysis. As discussed in sections 4 and 5, the irreversible dispersion κ_{irrev} is useful for comparing the observed tracer dispersion along isopycnal surfaces to a variety of theoretical models, including vertical shear dispersion.

1.2. Goals and Outline

The present study focuses on two main questions: (1) What are the rates of lateral dispersion over the continental shelf on spatial scales of 1–10 km and timescales of <5 days? (2) What are the mechanisms that determine these rates?

In section 2 we describe the field program of the CMO dye studies. In section 3 we estimate rates of lateral dispersion for each of the dye experiments using a simple model of vertical and horizontal shears and strains. In sections 4 and 5 we examine two existing paradigms of lateral dispersion, vertical shear dispersion and dispersion by lateral intrusions. In general, these mechanisms cannot account for the small-scale lateral dispersion observed during the CMO dye studies. In section 6 we discuss the implications of these results and suggest an alternative mechanism, dispersion by vortical motions caused by the relaxation of diapycnal mixing events, which may explain the observations. In section 7 we summarize the important results of this work and discuss outstanding questions.

2. Overview of the Field Program

The CMO dye studies were performed ~100 km south of Martha's Vineyard, Massachusetts, in the region known as the "Mud Patch." Five dye experiments were performed near the 70 m isobath, between the alongshore and central CMO mooring sites. The experiment dates and injection locations are given in Table 1. Of the five dye experiments conducted, four were performed at middepths and are examined in the present study. The fifth experiment was performed near the bottom boundary layer and is discussed by J. R. Ledwell et al. (manuscript in preparation, 2000).

For each experiment, dye was released in a single streak along a target isopycnal surface using a towed injection system. Three to six drogues were released along with the dye at the target depth and tracked via Argos transmitters that were tethered to the drogues. The drogue positions were used along with near real-time shipboard acoustic Doppler current profiler (ADCP) observations both to assist in locating the dye patch and as an aid to planning sampling strategies during the dye surveys. A detailed description of the injection and sampling survey techniques are given by J. R. Ledwell et al. (manuscript in preparation, 2000).

After each injection, three-dimensional surveys of the dye patch were conducted using a sampling sled that was tow-yo'd behind the ship at 2–4 kts. During these surveys the winch operated at speeds between 30 and 60 m min^{-1}, providing a vertical profile every 100–200 m along the ship track. The sampling system included either a rhodamine or fluorescein fluorometer, a chlorophyll fluorometer, and a Seabird conductivity-temperature-depth profiler (CTD). These instruments sampled at rate of 6 Hz, providing an average vertical resolution of 10 cm.

In each experiment, two to three surveys of the dye patch were conducted over the 2.5–5 days following the injection. Each survey consisted of between 3 and 33 transects through the patch. The first survey of each experiment generally yielded the fewest transects (ranging from 3 to 11) since at these times the patch was smallest and most difficult to track. The final survey of each experiment yielded between 9 and 33 transects through the patch. From the 4 experiments examined here, 9 out of 11 surveys appeared to resolve the dye patch (i.e., provide at least 10 transects through the patch) and delimit its boundaries [*Sundermeyer*, 1998].

For each of the dye surveys, tow-yo casts were "snipped" into individual up and down profiles, and a horizontal position for each profile was computed as its distance from the starting point of the dye injection. A Lagrangian correction was then applied to these positions using the integrated ADCP velocity at the target depth. This was done to account for the advection of

Table 1. Overview of Dye Experiments Performed During CMO

	Dates	Dye	Injection Latitude, Longitude	Target σ_θ, kg/m^3	Target depth, m	Surveys
Experiment 1	Sept. 11–14, 1995	rhodamine	40.44°N, 70.49°W	25.20	40	2
Experiment 2	Sept. 6–10, 1996	rhodamine	40.46°N, 70.32°W	24.063	35	3
Experiment 3	Sept. 12–16, 1996	fluorescein	40.47°N, 70.32°W	24.30	46	3
Experiment 4	Aug. 1–6, 1997	rhodamine	40.48°N, 70.33°W	24.6	18	3
Experiment 5	Aug. 7–12, 1997	fluorescein	40.48°N, 70.49°W	26.14	62	3

the dye patch during the course of each survey. Next, dye concentration was computed as a function of potential density and then transformed back into a vertical distance coordinate using the mean potential density versus pressure relationship averaged over each survey. This was done to remove the heaving of isopycnals due to internal waves while retaining a vertical distance coordinate, which could be used in computing vertical diffusivities.

2.1. Vertically Integrated and Target Surface Tracer

For each survey the method of ordinary kriging was used to generate maps of the dye patch in the horizontal plane [*Journel and Huijbregts*, 1978; see also *Ledwell et al.*, 1998]. Both the vertically integrated tracer and the tracer along the target density surface were interpolated onto a regular grid along with their associated mapping error fields. Kriging maps for the vertically integrated tracer for each of the four experiments are shown in Plate 1. (Maps for the tracer along the target density surface are not shown.) In all cases the dye patches grew significantly over the course of the experiment, spreading from their initial streak length of 1 km to patches as much as 20 km in length. Invariably, the spreading was anisotropic, with the major axis of the patch as much as 5 times the length of the minor axis (e.g., experiment 4). In some cases (such as experiment 3) the patches were also subject to considerable advection (speeds exceeding 10 cm s^{-1}).

From each of the above kriging maps the first three horizontal moments of the tracer, i.e., total mass, center of mass, and variance, were computed along with their uncertainties using the method described by *Ledwell et al.* [1998]. These moments form the basis of our analysis. For the vertically integrated tracer $\zeta(x,y)$ the moments are defined as follows:

$$M_{pq} = \int_{-\infty}^{+\infty}\int_{-\infty}^{+\infty} x^p y^q \zeta(x,y)\,dx\,dy. \tag{1}$$

The moments of interest relative to the center of mass of the tracer are

Total tracer $$M = M_{00}, \tag{2a}$$

Zonal center of mass $$X_{\text{com}} = M_{10}, \tag{2b}$$

Meridional center of mass $$Y_{\text{com}} = M_{01}, \tag{2c}$$

Zonal variance $$\sigma_x^2 = \frac{M_{20} - M_{10}^2}{M}, \tag{2d}$$

Meridional variance $$\sigma_y^2 = \frac{M_{02} - M_{01}^2}{M}, \tag{2e}$$

Zonal-meridional covariance $$\sigma_{xy} = \frac{M_{11} - M_{10}M_{01}}{M}. \tag{2f}$$

For a Gaussian distribution that is oriented at some angle ϕ with respect to the zonal-meridional axes the second moments above, i.e., the variances, can equivalently be expressed in terms of the variances along the major and minor axes:

Variance along the major axis

$$\sigma_a^2 = \frac{1}{2}\left[\sigma_x^2 + \sigma_y^2 + \frac{\sigma_{xy}}{\cos(\phi)\sin(\phi)}\right], \tag{3a}$$

Variance along the minor axis

$$\sigma_b^2 = \frac{1}{2}\left[\sigma_x^2 + \sigma_y^2 - \frac{\sigma_{xy}}{\cos(\phi)\sin(\phi)}\right], \tag{3b}$$

Angle of rotation $$\phi = \frac{1}{2}\arctan\left(\frac{2\sigma_{xy}}{\sigma_x^2 - \sigma_y^2}\right). \tag{3c}$$

Horizontal moments along the target density surface are exactly analogous, except that the vertically integrated tracer in (1) is replaced by the tracer concentration along the target density surface $\theta(x,y)$. In the interest of clarity the notation summarized in Table 2 will be used to distinguish between the former and the latter.

The variances $\tilde{\sigma}_a^2$ and $\tilde{\sigma}_b^2$ for each experiment were computed using the kriging maps of the vertically integrated tracer (Plate 1) and are summarized in Figure 2. Similar plots of the variances σ_a^2 and σ_b^2 for tracer along the target density surface are also shown in Figure 2. As was expected for a tracer that is being vertically sheared, the variances of tracer along the target density surface were smaller than those computed from the vertically integrated tracer. For both measures of variance a wide range of patch growth rates can be seen among the different experiments.

3. Estimates of Lateral Dispersion

In order to evaluate the rates of dispersion from the CMO dye studies the moments defined in section 2 were used in conjunction with a simple strain-diffusion model, which takes into account what we believe were the dominant processes acting on the dye patch. Using this model, the growth of the horizontal patch variances was computed using both the vertically integrated tracer and the tracer along the target density surface. The resulting diffusion parameters provide a measure of the total and the irreversible dispersion of the dye.

3.1. A Strain-Diffusion Model

In light of the observed elongation of the tracer patches (Plate 1) and the analysis of patch variances of section 2.1 we assume a simple model to describe the evolution of the tracer patches. Namely, we assume that the growth of the horizontal patch variances is controlled by an effective horizontal diffusivity plus a large-scale horizontal strain, $\gamma = \frac{\partial u}{\partial x} = -\frac{\partial v}{\partial y}$.

For a two-dimensional linear strain γ and a constant, isotropic horizontal diffusivity κ the advection-diffusion equation for a tracer C can be written as

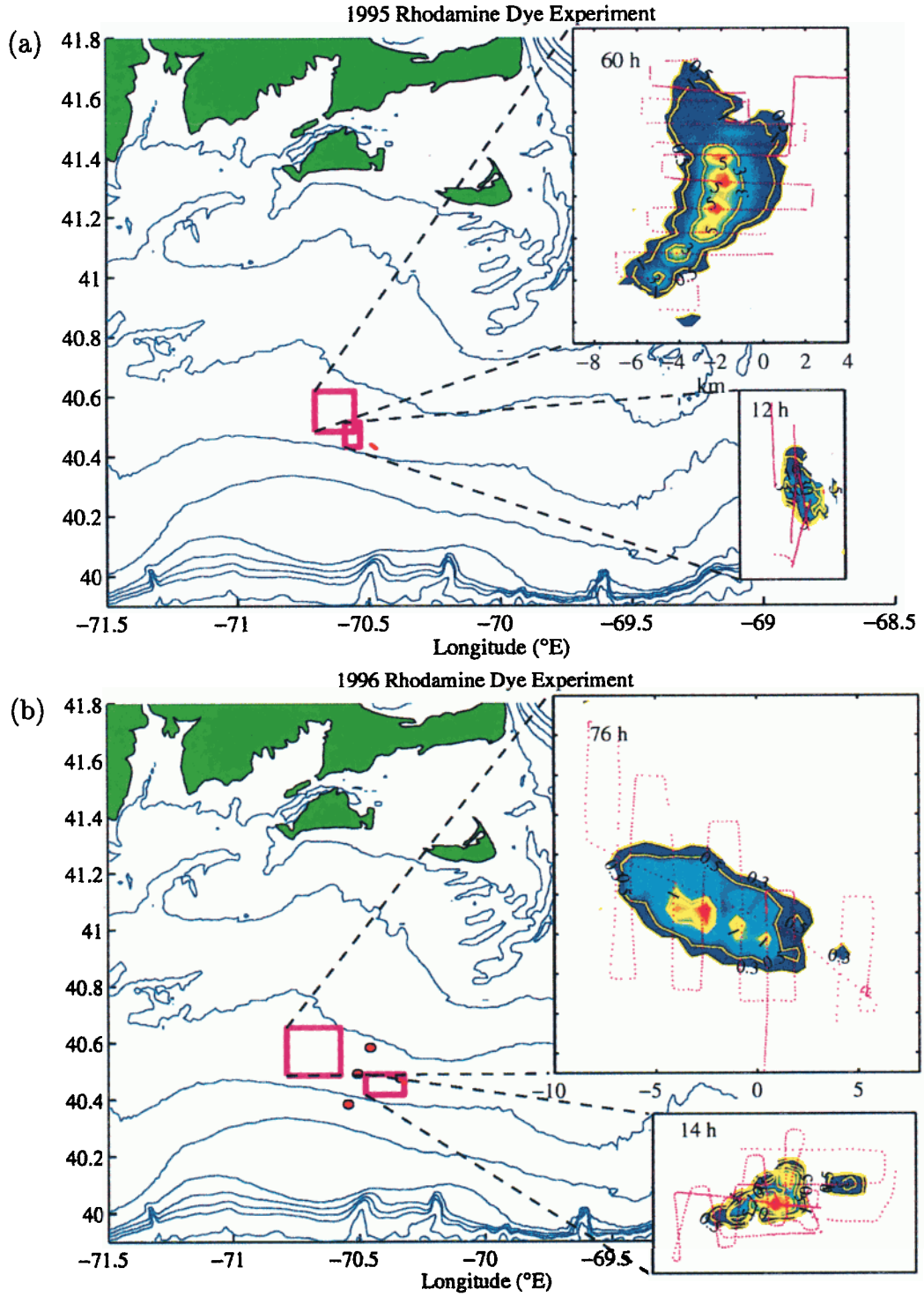

Plate 1. Summary of experiments 1–4 of the CMO dye studies. Insets show kriging maps of the vertical integral of tracer (kg km^{-2}) overlaid by the ship track (dotted line). Times for each survey relative to the injection time are shown in their respective panels. The relative locations of the dye patches to the CMO moorings during each of the surveys are indicated by boxes. Horizontal scales are the same in all the insets.

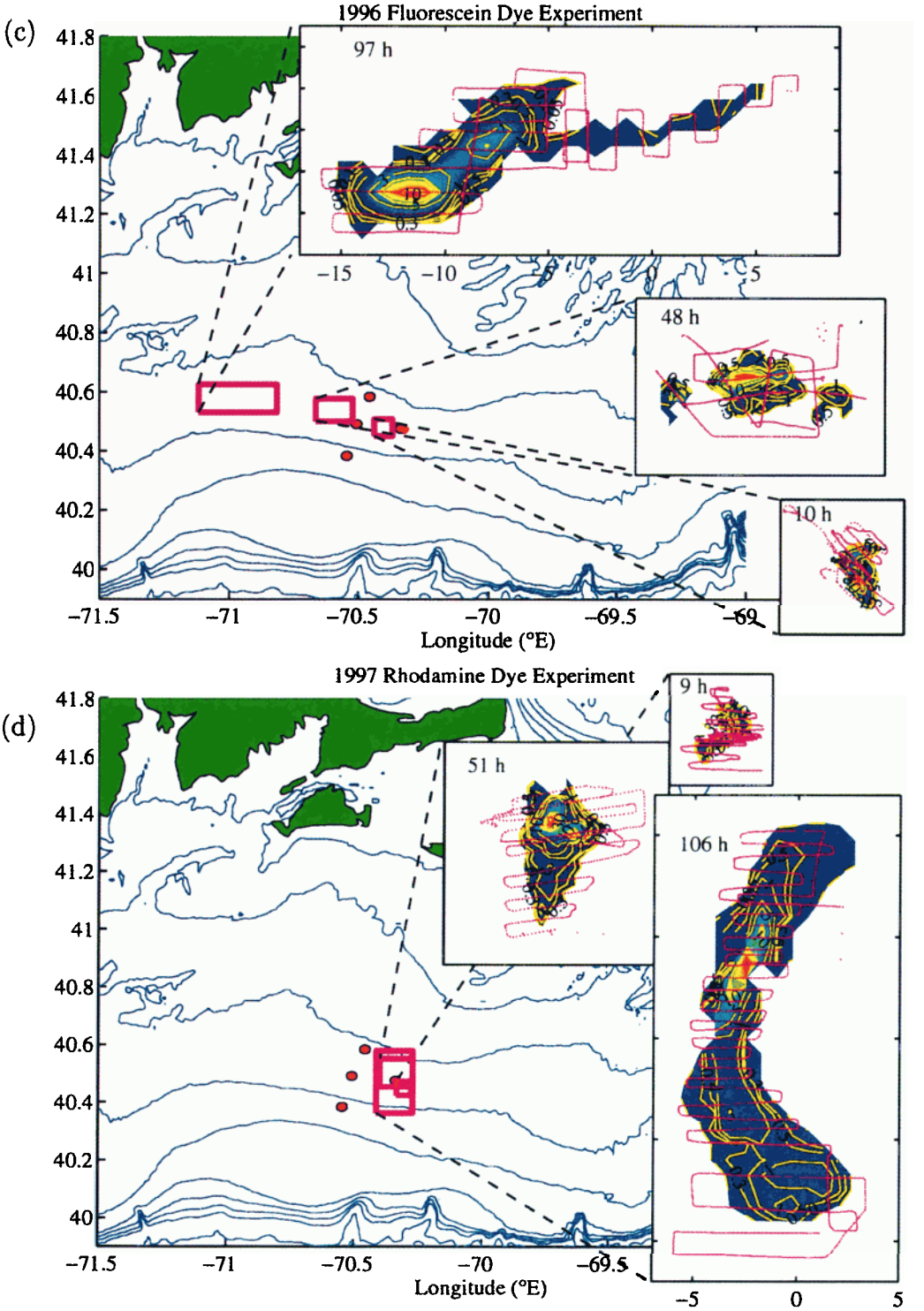

Plate 1. (continued)

$$\frac{\partial C}{\partial t} + \gamma x \frac{\partial C}{\partial x} - \gamma y \frac{\partial C}{\partial y} = \kappa \frac{\partial^2 C}{\partial x^2} + \kappa \frac{\partial^2 C}{\partial y^2}. \quad (4)$$

Multiplying by x^2 and integrating over all x, or by y^2 and integrating over all y, equations for the tracer variances σ_a^2 and σ_b^2 in the directions of the major and minor axes are [e.g., *Townsend*, 1951]

$$\frac{d\sigma_a^2}{dt} - 2\gamma\sigma_a^2 = 2\kappa, \quad (5)$$

$$\frac{d\sigma_b^2}{dt} + 2\gamma\sigma_b^2 = 2\kappa, \quad (6)$$

respectively, with solutions

$$\sigma_a^2 = \sigma_{ao}^2 e^{2\gamma t} + e^{2\gamma t} \int_0^t 2\kappa e^{-2\gamma t} dt, \quad (7)$$

$$\sigma_b^2 = \sigma_{bo}^2 e^{-2\gamma t} + e^{-2\gamma t} \int_0^t 2\kappa e^{2\gamma t} dt. \quad (8)$$

Using a reference frame in which the origin moves with the center of mass of the dye and the x and y axes are aligned with the major and minor axes of the patch, respectively, this model can be applied to both the vertically integrated tracer $\zeta(x,y)$ and the tracer along the target density surface $\theta(x,y)$ to obtain estimates of the effective total diffusivity κ_ζ and the effective irreversible diffusivity κ_{irrev}.

Noteworthy in the above strain-diffusion model are the assumptions that the large-scale strain field is steady and horizontally uniform, and that smaller-scale variations in the strain rate (scales less than or equal to the scale of the dye patch) can be parameterized by an effective small-scale diffusivity. This approach follows the early ideas of *Taylor* [1921] regarding the parameterization of small-scale stirring as an effective small-scale diffusive process, and is also consistent with the idea of scale-dependent diffusion [e.g., *Okubo*, 1971]. (The presence of small-scale variations in the strain rate might be assessed in a statistical sense from higher moments of the dye patches. However, the coarse temporal resolution of the sampling surveys would limit any quantitative deterministic measure of such small-scale strains. We have also found shipboard ADCP data to be of limited use in assessing such strains because of the problem of distinguishing spatial variability from temporal variability on the appropriate scales. Whether the horizontal scale of the strain field could be further constrained using data from the CMO moored current meter array deployed by S. Lentz, A. Plueddeman, S. Anderson, and J. Edson has not been investigated here and is left as a subject for future investigation.)

3.2. Estimates of κ_ζ and κ_{irrev}

Using the horizontal variances estimated in section 2.1 and the simple strain-diffusion model described in section 3.1, a large-scale strain rate and effective horizontal diffusivity for each experiment can be estimated as follows. Consider first the vertically integrated tracer. Given an initial and final along-streak variance (i.e., some measure of the spread of tracer along the major axis of the dye patch), (7) implies that if the strain rate $\tilde{\gamma}$ is known, then the along-streak diffusivity κ_ζ can be inferred or vice versa. Put another way, for a given initial condition, (7) indicates the combinations of $\tilde{\gamma}$ and κ_ζ that could explain the observed final along-streak variance; a larger value of $\tilde{\gamma}$ implies a smaller value of κ_ζ and vice versa. This range of combinations can be expressed as a negative-sloping curve in a two-dimensional $\tilde{\gamma}$-κ_ζ parameter space (Figure 3). For a different final condition a different curve will result; the larger the final condition, the farther the curve will be shifted toward larger $\tilde{\gamma}$ or larger κ_ζ. A different initial condition will lead to a different family of curves. For example, a smaller initial condition requires a larger $\tilde{\gamma}$ or a larger κ_ζ to yield the same final condition.

Similar reasoning can be applied to the cross-streak direction using (8). In that case a larger strain rate, i.e., more negative in the cross-streak direction, requires a larger diffusivity to maintain the same patch width so that the curves have a positive slope. The larger the final condition, the farther the curves will be shifted toward smaller $\tilde{\gamma}$ or larger κ_ζ.

Using these families of curves, the strain rate $\tilde{\gamma}$ and the small-scale diffusivity κ_ζ for each experiment can be estimated from the intersections of the along- and cross-streak curves. The results of this analysis, as well as similar results for the tracer along the target den-

Table 2. Notation Used in Discussion of Horizontal Dispersion

Description of Variable	Notation for Vertically Integrated Tracer	Notation for Tracer Along Target Density Surface
Dye concentration	$\zeta = \zeta(x,y)$	$\theta = \theta(x,y)$
Variances along major and minor axes, and angle of rotation	$\tilde{\sigma}_a^2, \tilde{\sigma}_b^2, \tilde{\phi}$	$\sigma_a^2, \sigma_b^2, \phi$
Horizontal strain rate	$\tilde{\gamma}$	γ
Effective horizontal diffusivity	κ_ζ	κ_{irrev}

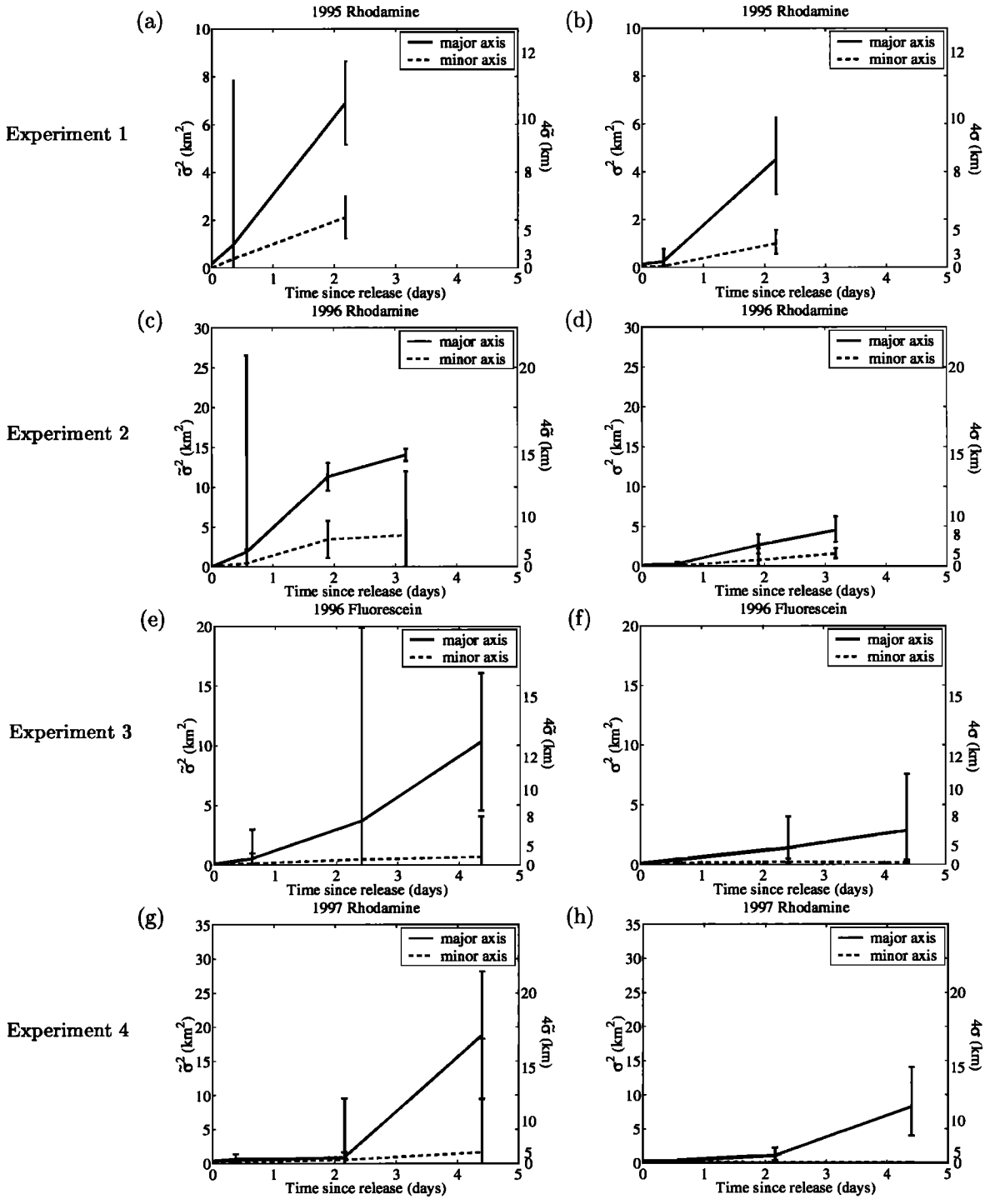

Figure 2. Patch variances along the major and minor horizontal axes estimated (a), (c), (e), and (g) from the vertically integrated tracer and (b), (d), (f), and (h) along the target density surface for the 1995, the 1996, and the first 1997 CMO dye experiments. Error bars were computed using the method described by *Ledwell et al.* [1998]. Note the different vertical scales.

sity surface, are listed in Table 3. Analogous curves in γ-κ_{irrev} space for the tracer along the target density surface are also shown in Figure 3.

For the vertically integrated tracer the inferred strain rate ranges from $\tilde{\gamma} = 2.3 \times 10^{-6}$ to 3.5×10^{-6} s^{-1}, while the diffusivity ranges from $\kappa_\zeta = 2.5$ to 12.7 m^2 s^{-1}. For the tracer along the target density surface the strain rate ranges from $\gamma = 1.9 \times 10^{-6}$ to 4.0×10^{-6} s^{-1}, and the diffusivity ranges from $\kappa_{irrev} = 0.3$ to 4.9 m^2 s^{-1}. Estimates of the large-scale horizontal strain rate show remarkably little variation among the four experiments. In addition, estimates of γ based on the tracer along the

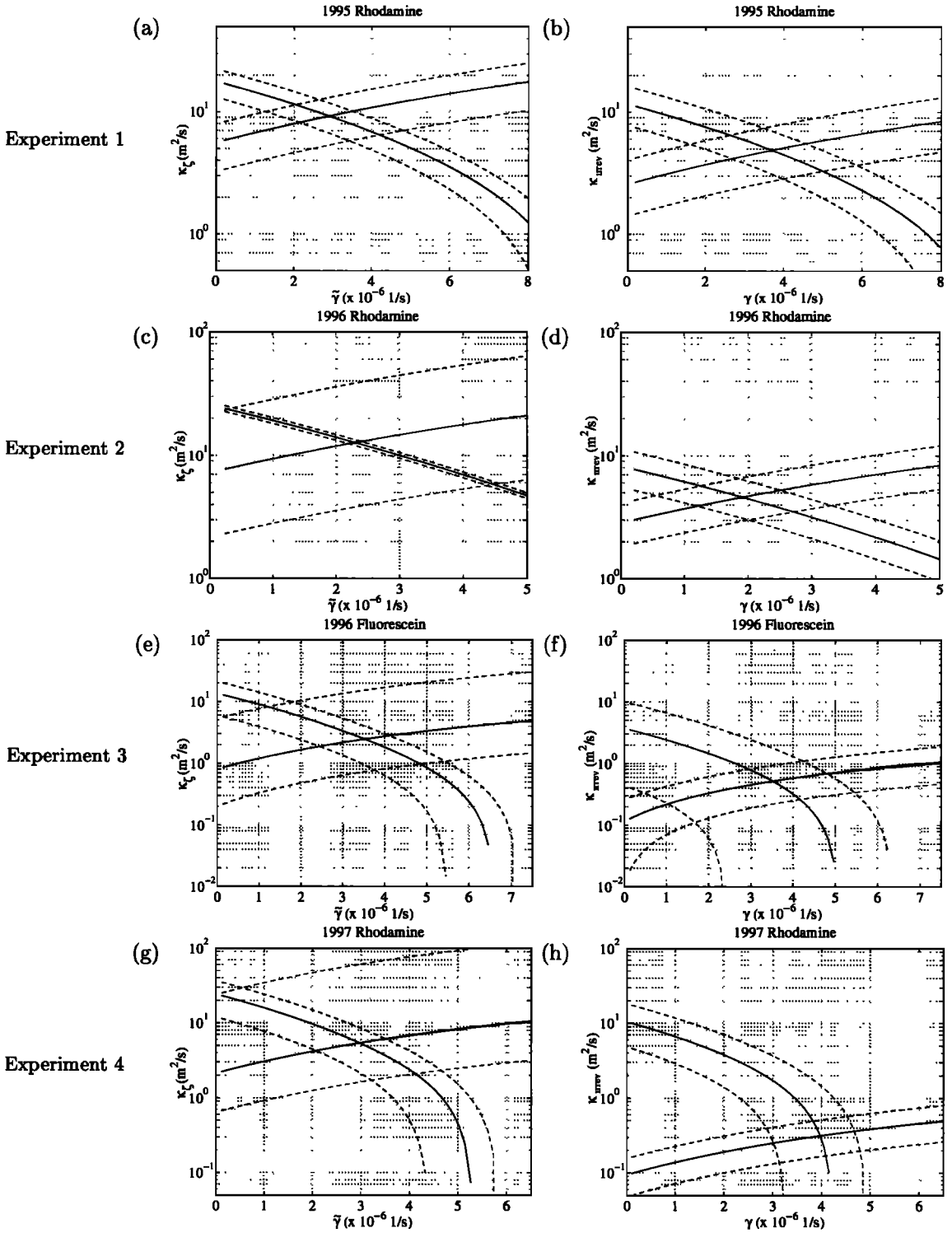

Figure 3. Graphic representation of (a), (c), (e), and (g) possible combinations of $\tilde{\gamma}$ and κ_ζ that could explain the observed growth of tracer variance for the vertically integrated tracer and (b), (d), (f), and (h) possible combinations of γ and κ_{irrev} for the tracer along the target density surface for the 1995, the 1996, and the first 1997 CMO dye experiments. Solid curves are the best estimates based on estimated variances computed in section 2.1, and dashed curves indicate uncertainties. The point of intersection of the two solid curves in each panel indicates our best estimate of γ and κ_{irrev}. (See also Table 3.)

Table 3. Horizontal Strain Rates $\tilde{\gamma}$ and γ and Horizontal Diffusivities κ_ζ and κ_{irrev} Estimated From the Vertically Integrated Tracer and From Concentration Along the Target Density Surface[a]

	$\tilde{\gamma} \times 10^{-6}$, s^{-1}	κ_ζ, $m^2\ s^{-1}$	$\gamma \times 10^{-6}$, s^{-1}	κ_{irrev}, $m^2\ s^{-1}$
Experiment 1	2.9 (1.3–4.8)	9.2 (5.8–12.6)	3.7 (1.6–5.8)	4.9 (2.9–7.3)
Experiment 2	2.3 (0.2–4.6)	12.7 (5.7–24.2)	1.9 (0.6–3.3)	4.6 (3.0–6.5)
Experiment 3	3.5 (0.2–5.4)	2.5 (0.7–9.8)	3.5 (0.5–5.4)	0.5 (0.1–1.1)
Experiment 4	3.0 (0.0–4.6)	5.4 (1.7–30.0)	4.0 (2.8–4.8)	0.3 (0.1–0.6)

[a]Uncertainties are given by the intersections of the upper bound and lower bound curves for the final patch variances. (See also Figure 3.)

target density surface are roughly consistent with $\tilde{\gamma}$ inferred from the vertically integrated tracer. However, estimates of κ_{irrev} are smaller (2–18 times) than the total effective diffusivity κ_ζ. The latter two points are consistent with our conceptual model described in section 3.1, i.e., that the overall (total) diffusivity κ_ζ represents the sum of some irreversible diffusivity κ_{irrev} plus a reversible component due to the vertical shear. The fact that the two estimates of the large-scale horizontal strain rate, γ and $\tilde{\gamma}$, are in agreement is consistent with the idea that these parameters represent the same horizontal straining process.

4. An Evaluation of Shear Dispersion

In the first part of the this paper we quantified rates of lateral dispersion over the continental shelf using the CMO dye studies. The rest of this paper is devoted to understanding the mechanisms responsible for this dispersion. Specifically, we focus on understanding the mechanisms responsible for the irreversible diffusivities κ_{irrev} since these by definition represent small-scale processes that were unresolved in the CMO observations and are the least understood.

A notable feature in all of the dye experiments performed during CMO was a dramatic change in the vertical tilt of the dye patch during successive surveys of the tracer, presumably due to a vertical shear (not shown) [see *Sundermeyer*, 1998]. In some cases the shear appeared to persist throughout the experiment, creating horizontal displacements as large as 2–5 km between the shallowest and deepest parts of the dye patch. In other cases the shear appeared to oscillate, reversing the tilt of the dye patch within the few hours it took to complete a single survey. These observations suggest that vertical shear dispersion is a natural candidate as a lateral dispersion mechanism in the CMO region. (Note that the presence of oscillatory shears also adds to the uncertainty of our estimates of vertically integrated dispersion κ_ζ.)

The role of vertical shear dispersion in the CMO dye studies is examined in this section. This analysis shows that shear dispersion cannot explain the observed irreversible lateral dispersion in the CMO dye experiments. Instead, some other mechanism is required to contribute an effective small-scale horizontal diffusivity of order 0.2–4.6 $m^2\ s^{-1}$.

4.1. Theoretical Background

As originally described by *Taylor* [1953] in his studies of pipe flow dispersion, the interaction between a longitudinal (i.e., horizontal) flow and a transverse (i.e., vertical) diffusivity can lead to an enhanced longitudinal diffusivity that is inversely proportional to the transverse diffusivity. This problem has been widely studied since Taylor's original work, with subsequent investigators considering a number of variations of the original pipe flow problem [e.g., *Elder*, 1959; *Chatwin*, 1975]. Taylor's ideas have also found much relevance in geophysical flows, including freshwater lakes, rivers, and estuaries and the coastal ocean [e.g., *Bowden*, 1965; *Csanady*, 1966].

One underlying assumption of the latter studies, which typically involved shallow or well-mixed waters, was that the timescale of the transverse diffusion was small compared to the advective timescale of the flow. Consequently, vertical gradients of tracer were mixed away before the longitudinal velocity could advect the tracer a significant distance. In that case the effective horizontal diffusivity is predicted to be inversely proportional to the vertical diffusivity (henceforth this is referred to as Taylor's limit).

As discussed by *Saffman* [1962], the inverse proportionality of Taylor's limit may not apply to an unbounded or semibounded fluid if the timescale of the transverse diffusivity is much larger than the advective timescale. Rather, in this case the longitudinal diffusivity is predicted to be directly proportional to the transverse diffusivity (henceforth, Saffman's limit).

An extensive treatment of shear dispersion that encompassed both the Taylor and Saffman limits in an unbounded fluid was given by *Young et al.* [1982]. Among their many insightful results they derived solutions for the effective horizontal dispersion in a vertical shear flow that varies sinusoidally in both time and depth, i.e., for a horizontal velocity $u(z,t)$ of the form

$$u(z,t) = \frac{\alpha}{m} \sin(mz) \cos(\omega t), \tag{9}$$

where m is the vertical wavenumber, ω is the frequency, and α is the shear amplitude. In this case the long-term growth of the horizontal tracer variance σ_x^2 can be expressed as

$$\frac{1}{2}\frac{d\sigma_x^2}{dt} = \kappa_x + \frac{\kappa_z \alpha^2}{2(\omega^2 + m^4\kappa_z^2)}, \tag{10}$$

where κ_x and κ_z are explicit horizontal and vertical diffusivities, respectively, and the second term on the right-hand side represents the effective horizontal diffusivity due to shear dispersion [*Young et al.*, 1982]. For large vertical wavenumbers, $m^2 \gg \omega/\kappa_z$, the shear dispersion term in (10) reduces to $\alpha^2/2m^4\kappa_z$, which represents Taylor's limit. For small vertical wavenumbers, $m^2 \ll \omega/\kappa_z$, the shear dispersion term becomes $\kappa_z\alpha^2/2\omega^2$, which represents Saffman's limit.

More generally, (10) shows that in an unbounded fluid, shear dispersion is most effective at low frequencies and low vertical wavenumbers. This means that for a given shear amplitude α and vertical diffusivity κ_z, taking $m = 0$ in (10) yields an upper bound on the contribution of shear dispersion to the growth in the horizontal variance. We now exploit this result.

An important point regarding (10) is that this result rigorously applies only as an average over an integral number of, or sufficiently many, periods and wavelengths. A more practical solution for the purposes of the present study, and one which holds for arbitrary time, was given by *Smith* [1982]. He solved the advection-diffusion equation exactly for the case of a linear shear (i.e., $m = 0$ in (9)) of arbitrary time dependence. In two dimensions the problem is expressed as

$$\frac{\partial C}{\partial t} + u(z,t)\frac{\partial C}{\partial x} = \kappa_x \frac{\partial^2 C}{\partial x^2} + \kappa_z \frac{\partial^2 C}{\partial z^2}, \tag{11}$$

where C represents the concentration of tracer, κ_x and κ_z are the explicit horizontal and vertical diffusion coefficients, and the horizontal velocity $u(z,t)$ now varies linearly with depth:

$$u = u_o(t) + z\alpha(t). \tag{12}$$

(The analogous problem in three dimensions was also solved by *Smith*, [1982], but will not be discussed here.)

As shown by *Smith* [1982], a greatly simplified solution to (11) may be obtained with the introduction of an advected horizontal coordinate,

$$X = x - \int_0^t u_o(t')dt' - zG(t). \tag{13}$$

The second term on the right-hand side of (13) represents advection by the mean flow, while the third term represents the vertical tilt of the tracer patch, characterized by a distortion factor G, which is yet to be determined. Applying this change of variables to (11) and noting that for a time-dependent linear shear a Gaussian initial condition yields a Gaussian solution, the solution of (11) can be written in the form

$$C = \frac{M}{2\pi\sigma_x\sigma_z} e^{\left[-\frac{X^2}{2\sigma_x^2} - \frac{z^2}{2\sigma_z^2}\right]}, \tag{14}$$

where M is the total mass of tracer and $\sigma_x^2(t)$ and $\sigma_z^2(t)$ are the horizontal and vertical variances, respectively. Substituting (13) and (14) into (11), the following expressions are obtained for the evolution of the horizontal and vertical variances and the distortion factor G:

$$\frac{1}{2}\frac{d\sigma_x^2}{dt} = \kappa_x + \kappa_z G^2, \tag{15}$$

$$\frac{1}{2}\frac{d\sigma_z^2}{dt} = \kappa_z, \tag{16}$$

$$\frac{dG}{dt} = \alpha(t) - \frac{2\kappa_z G}{\sigma_z^2}. \tag{17}$$

Given a shear $\alpha(t)$ of arbitrary time dependence and diffusivities κ_x and κ_z, this system of ordinary differential equations (ODEs) can be solved exactly:

$$\sigma_x^2 = \sigma_{x_o}^2 + 2\kappa_x t + 2\kappa_z \int_0^t G^2 dt', \tag{18}$$

$$\sigma_z^2 = \sigma_{z_o}^2 + 2\kappa_z t, \tag{19}$$

$$G = \frac{1}{t - \tilde{t}} \int_0^t (t' - \tilde{t})\alpha(t')dt' \qquad (\tilde{t} = -\frac{\sigma_{z_o}^2}{2\kappa_z}). \tag{20}$$

The last term on the right-hand side of (18) represents the effective horizontal diffusivity due to shear dispersion and is analogous to the second term on the right-hand side of (10) in the limit of $m = 0$. Equation (20) shows that the distortion factor G represents a weighted mean shear or, effectively, a measure of the vertical tilt of the center of mass of the tracer patch. It is also noteworthy that the vertical variance (19) does not depend on the vertical shear. A schematic of the linear dispersion model is shown in Figure 4.

4.2. Comparison With Observations

The above theoretical ideas suggest that a linear shear ($m = 0$ in (10)) yields an upper bound on lateral dispersion due to shear dispersion. Equations (18)–(20) further provide an exact solution for the evolution of a passive tracer in the presence of a linear shear of arbitrary time dependence. We now use these solutions to determine upper bounds on the contribution of shear dispersion to the lateral dispersion observed during the CMO dye studies. Two questions are addressed: (1) What are the relative contributions of shear dispersion by mean, inertial, diurnal, and semidiurnal shears? (2) Can the total contributions of shear dispersion as esti-

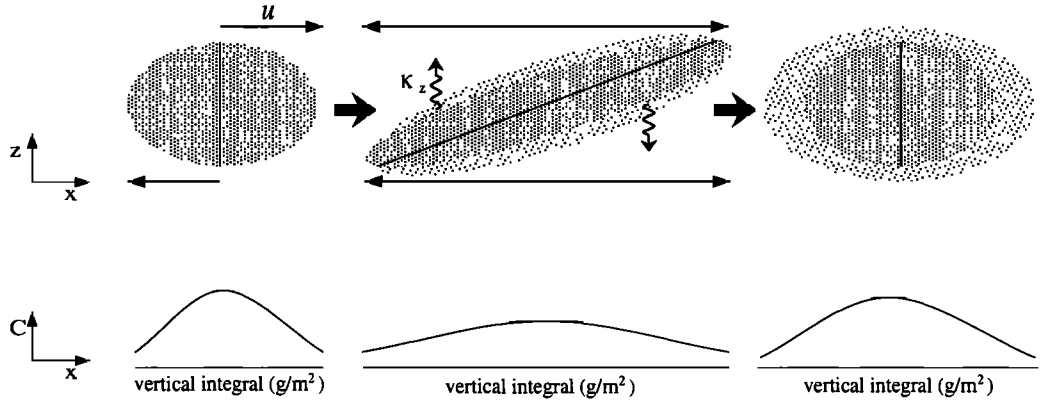

Figure 4. Schematic of linear shear dispersion model showing a dye patch that undergoes tilting by a vertical shear at the same time that it is being vertically diffused. The net effect, shown at the far right, is an effective horizontal dispersion that remains even after the advection is reversed.

mated using the full time series of ADCP shears explain the observed lateral dispersion in these experiments? The main result of this analysis is that in at least two of the dye studies examined, shear dispersion cannot explain the observed irreversible dispersion.

To determine the effectiveness of shear dispersion in each of the dye experiments, we solve (18)–(20) numerically using the shear at the mean depth of the target density surface. Here we use two forms of the ADCP time series: the raw ADCP record and a smoothed version (MIDS) based on harmonic analysis using a mean (M) plus oscillatory shears with inertial (I), diurnal (D), and semidiurnal (S) frequencies. In this we assume that the observed shear does not vary significantly in the horizontal, so that the shear measured by the ADCP represents the shear over the entire dye patch.

For each experiment, effective diffusivities for each of the harmonic constituents (mean, inertial, diurnal, and semidiurnal shears) are first computed individually on the basis of steady state solutions to (18)–(20); that is,

$$\kappa_M = \kappa_z \frac{\alpha_M}{2}(t - t_o), \tag{21}$$

$$\kappa_{[I,D,S]} = \kappa_z \frac{\alpha^2_{[I,D,S]}}{\omega^2_{[I,D,S]}}. \tag{22}$$

(Note that for convenience of notation we have written the contribution by mean shear in terms of an effective diffusivity. However, since a steady shear leads to a quadratic rather than a linear growth in tracer variance, the use of a Fickian diffusion parameterization is not strictly valid for this term.) Next, the full smoothed harmonic analysis time series, MIDS, and the raw ADCP time series are used to compute the full effective diffusivities for each experiment. Again, this is done by numerically integrating (18)–(20) for the length of each experiment. In all cases, integration was started from our maximum estimate of the initial conditions based on the observations, $\sigma^2_{x_o} = \sigma^2_{y_o} = 0.25$ km^2 ($4\sigma_x = 4\sigma_y = 2$ km) and $\sigma^2_{z_o} = 0.39$ m^2 ($4\sigma_z = 2.5$ m) [*Sundermeyer*, 1998; J. R. Ledwell et al., manuscript in preparation, 2000]. Upper bounds on the vertical diffusivities κ_z were used, thus reinforcing that these predictions represent upper bounds on shear dispersion. The results of this analysis are shown in Figure 5, and listed in Table 4. (An analysis of vertical diffusivities based on the dye studies is given by J. R. Ledwell et al. (manuscript in preparation, 2000). Values of κ_z that were taken from their analysis and used in the present study are κ_z = (1.5, 3.0, 0.9, and 0.4) $\times 10^{-5}$ m^2 s^{-1} for experiments 1–4, respectively.)

Comparing the results for the harmonically fit time series, the four experiments show a wide range of irreversible diffusivities, with values ranging from κ_{MIDS} = 0.003 to 1.3 m^2 s^{-1}. Among the indvidual harmonic constituents, mean shear dispersion (M) generally dominated oscillatory shear dispersion and was frequently 2–3 orders of magnitude larger than any of the oscillatory components (I, D, and S). It is also noteworthy that in some cases, oscillatory shear dispersion was dominated by inertial oscillations, while in others, it was dominated by tidal oscillations. The shear dispersion predictions using the full ADCP time series gave results similar to those of the harmonically fit time series.

Comparing the shear dispersion predictions from both the harmonically fit and the full ADCP time series, i.e., κ_{MIDS} and κ_{ADCP}, to the effective irreversible diffusivities, κ_{irrev} estimated from the observations (Tables 3 and 4), we find that in all cases, shear dispersion underpredicts the observed dispersion. This is an interesting result in that it suggests that another mechanism must have contributed significantly to the effective small-scale diffusivity during the CMO dye experiments. Most notably, the analyses of the 1995 and 1996 rhodamine dye studies suggest that some other mechanism must have contributed an additional horizontal diffusivity of $\kappa_{\text{missing}} \approx 2.9$–$4.6$ m^2 s^{-1}. The observed horizontal diffusivity in the 1996 fluorescein and the 1997 rhodamine experiments was somewhat smaller,

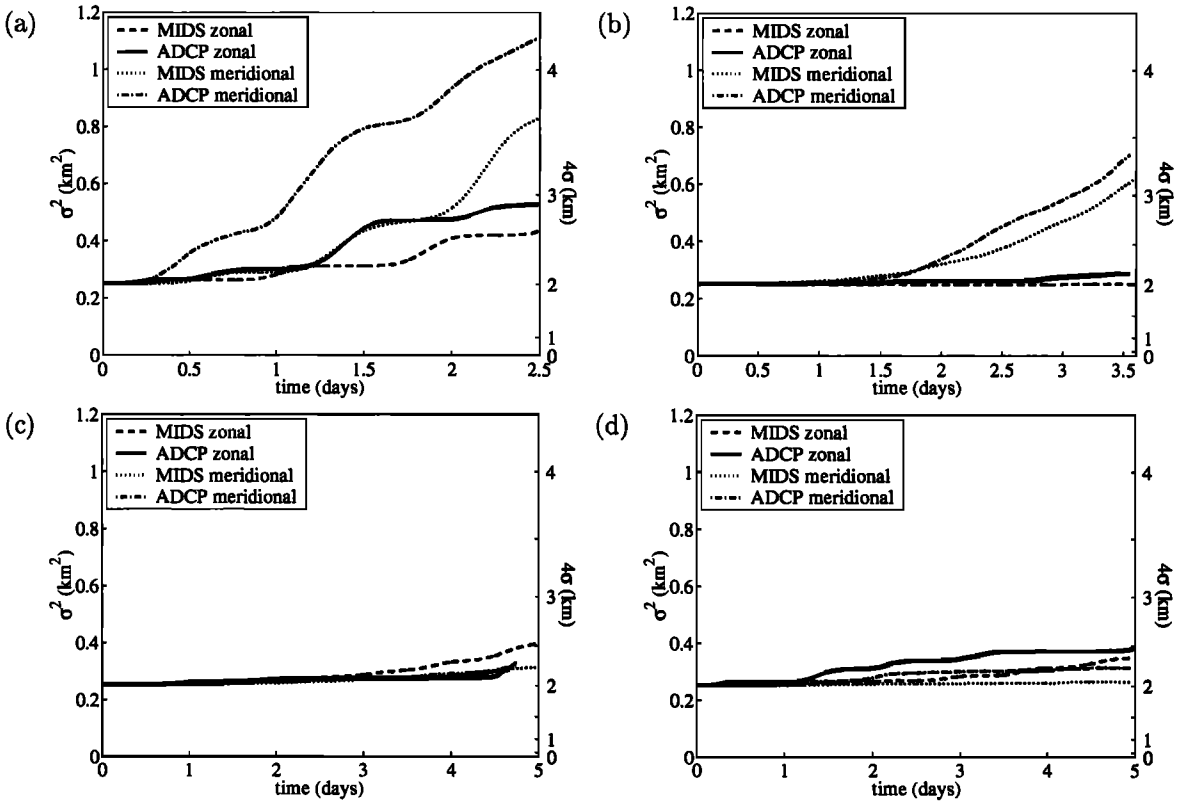

Figure 5. Theoretical predictions for zonal and meridional shear dispersion in the (a) 1995, (b)–(c) 1996, and (d) 1997 dye studies based on numerical integration of (18)–(20) and horizontal and vertical diffusivities estimated from the observations. Dashed curves are for a mean plus inertial, diurnal, and semidiurnal (MIDS) shears as estimated from a least squares fit to the ADCP data. Solid curves are for the full ADCP time series. (See also Table 4).

with an additional diffusivity required in those cases of $\kappa_{missing} \approx 0.2$–$0.4$ m^2 s^{-1}.

That shear dispersion cannot explain the observed lateral dispersion in the CMO dye experiments is one of the most important results of this study. It suggests that on timescales of a few days and spatial scales of 1–10 km some other mechanism contributes significantly to lateral dispersion over the continental shelf. On the basis of the above calculations, it could be argued that shear dispersion can explain the observed dis-

Table 4. Theoretical Predictions of Effective Horizontal Diffusivity by Shear Dispersion in the 1995, 1996, and 1997 Dye Studies; Horizontal Diffusivities Computed From the observations; and Estimated Missing Diffusivities[a]

		κ_M, m^2 s^{-1}	κ_I, m^2 s^{-1}	κ_D, m^2 s^{-1}	κ_S, m^2 s^{-1}	κ_{MIDS}, m^2 s^{-1}	κ_{ADCP}, m^2 s^{-1}	κ_{irrev}	$\kappa_{missing}$
Experiment 1	zonal	0.23	0.17	2.4×10^{-3}	4.3×10^{-3}	0.43	0.65	4.9	2.9–4.5
	meridional	0.93	0.12	1.1×10^{-2}	4.9×10^{-3}	1.3	2.0		
Experiment 2	zonal	0.002	3.3×10^{-4}	2.6×10^{-4}	2.0×10^{-4}	0.003	0.06	4.6	3.9–4.6
	meridional	0.55	1.5×10^{-3}	7.0×10^{-4}	1.0×10^{-3}	0.60	0.73		
Experiment 3	zonal	0.14	9.9×10^{-3}	2.5×10^{-3}	3.7×10^{-5}	0.17	0.09	0.5	0.3–0.4
	meridional	0.05	6.6×10^{-3}	1.4×10^{-3}	7.7×10^{-4}	0.07	0.08		
Experiment 4	zonal	0.07	1.1×10^{-2}	2.2×10^{-3}	1.2×10^{-3}	0.12	0.15	0.3	0.2–0.3
	meridional	0.005	4.2×10^{-3}	8.7×10^{-3}	8.0×10^{-4}	0.018	0.077		

[a]Individual predictions are for harmonic analysis results for a mean shear (M), inertial oscillations (I), and diurnal (D) and semidiurnal (S) tides; the full harmonically fit time series (MIDS); and the raw shipboard ADCP time series. (See also Figure 5.)

persion in the 1997 rhodamine dye experiment since at least the zonal shear dispersion prediction lies within the uncertainty of observed dispersion estimates (see Table 3). However, since the shear dispersion estimates represent upper bounds as described at the beginning of this section and since the κ_{missing} therefore represent lower bounds on the missing diffusivities, we consider this unlikely.

The above result is strengthened further if we consider the effects of a time dependent vertical diffusivity $\kappa_z = \kappa_z(t)$, which is approximately in phase with the shear amplitude (as would be the case for shear instability). In this case, $\kappa_z(t)$ would be in quadrature with the shear displacements. For a fixed value of the mean vertical diffusivity, this would lead to a reduction in the lateral dispersion due to shear dispersion. For a two-dimensional vertical shear it is possible that the phase difference between the vertical diffusivity and the displacement could reduce shear dispersion in one direction while enhancing it in the other. However, this effect would only be significant if there were significant anisotropy in the vertical shears, which for the CMO region was not the case [*Sundermeyer*, 1998].

A final note regarding the above results is that predictions of shear dispersion are most appropriately made using the shear across an isopycnal surface rather than at a fixed depth. This distinction may be important if the depth of the target density surface varies significantly over the course of an experiment. On the basis of analysis of shipboard ADCP data in conjunction with CTD data from the dye surveys, the depth of the target density surface fluctuated as much as 15 m about its mean level. To assess the significance of this variation, a detailed case study of the 1995 rhodamine experiment was performed. This showed that the shear dispersion prediction was not altered significantly when the shear across the target density layer was used rather than the shear at a fixed depth [*Sundermeyer*, 1998]. Such analysis was not possible for all the experiments because CTD data were not available at all times to track the depth of the target density surface. However, given the extent of our analysis, the main conclusion of this section is unaffected; shear dispersion cannot explain the observed lateral dispersion in the CMO dye studies.

5. Lateral Intrusions

In section 4 we showed that shear dispersion alone, even with a time-dependent vertical diffusivity and an appropriate shear across the target density layer, does not account for the observed lateral diffusion of the dye. We now consider mixing by lateral intrusions as a second potential mechanism that may account for the observed dispersion. Two classes of intrusions are examined: large-scale water mass intrusions such as those described by *Stommel and Fedorov* [1967] and diffusive interleaving such as discussed by *Stern* [1967]. The main result of this analysis is that dispersion by lateral intrusions also cannot explain the observed lateral dispersion in the CMO dye studies.

5.1. Large-Scale Intrusions

As discussed, for example, by *Stommel and Fedorov* [1967] horizontal density gradients can cause interleaving density currents that lead to large-scale water mass intrusions. These occur when the density of a water mass at one location is intermediate relative to density layers at a neighboring location. Given the proximity of the shelf-slope front to the CMO study site, it is not surprising that evidence of such intrusions can be seen in data collected during the CMO dye experiments. Plate 2 shows an example of one such intrusion observed during the final survey of the 1995 pilot dye study.

The transect shows a mass of warm, saline water ($\sigma \approx$ 25.1–25.5) intruding toward the west (right to left), starting approximately from where the ship's log marks 3 km along the transect. The intrusion is centered at a depth of about 40–50 m, has a vertical scale of 5–10 m, and has a horizontal scale of a few kilometers. Horizontal temperature gradients as large as 2^{o}C km^{-1} and salinity gradients as large as 1 psu km^{-1} are associated with this intrusion.

Consider the effect of such an intrusion on the dye patch. Here relative size is a key factor. Both the vertical and horizontal scales of the intrusion were comparable to the scales of the tracer patch. Thus the pressure gradients driving the intrusion could be expected to have had the same advective influence on the dye as they did on the density field. In other words, an intrusion of this magnitude would have differentially advected the dye patch in either the horizontal or vertical direction, or both. In the vertical direction, differential advection on these scales (5–10 m) would have been resolved by our ADCP observations as a vertical shear and would already have been incorporated in the shear dispersion calculations of section 4. In the horizontal direction these pressure gradients would have been the driving force for the large-scale horizontal shears and strains that elongated the patch in either the zonal or meridional direction. We therefore suggest that such a large-scale intrusion (relative to the size of the dye patch) should be considered an advective rather than a diffusive mechanism in the context of the present work, and thus would not explain the irreversible diffusivities estimated in section 3.

5.2. Diffusive Interleaving

As first discussed by *Stern* [1967], horizontal gradients in temperature and salinity may result in interleaving of water masses even in the absence of large-scale horizontal density gradients. This diffusive interleaving occurs when relatively warm/salty water lies next to cold/fresh water. Even when both water masses are stably stratified, a small horizontal displacement of one water mass into the other can create a region which

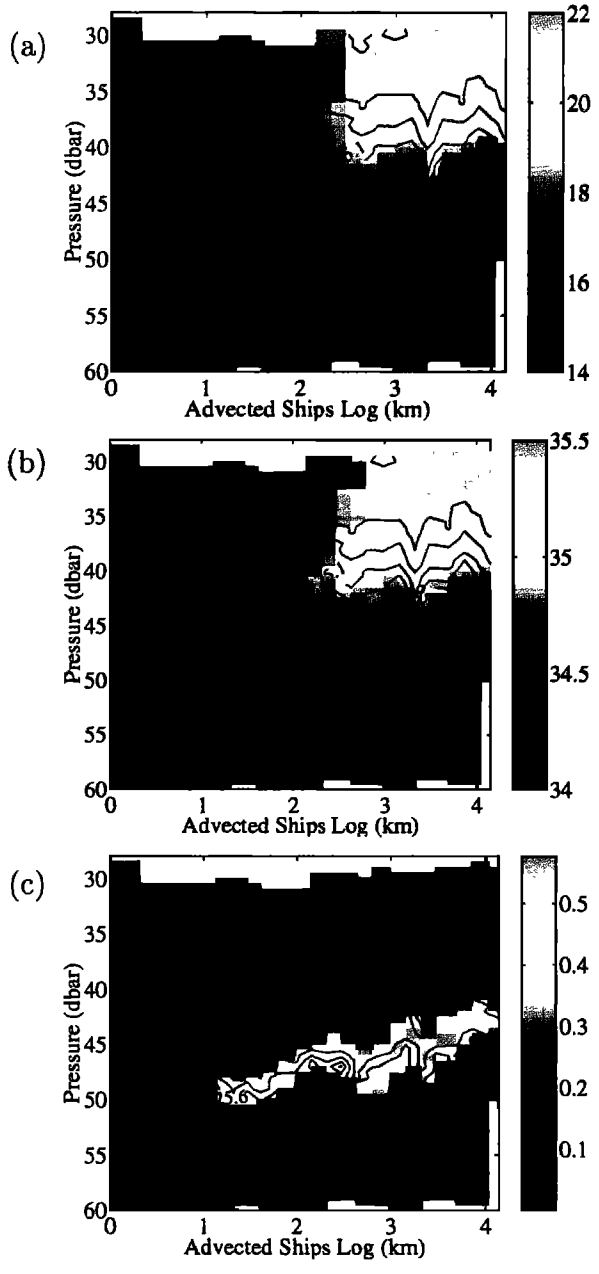

Plate 2. (a) Temperature and (b) salinity sections and (c) dye concentration along a zonal transect taken during survey 2 of the 1995 rhodamine dye study showing evidence of a large-scale T-S intrusion in the vicinity of the dye patch. Overplotted on each panel are contours of potential density in units of kg m^{-3}.

is double-diffusively unstable. The ensuing double diffusion may then cause a net salt (and buoyancy) flux, which leads to a local pressure gradient and then to further intrusion. This positive feedback mechanism results in a growing instability in which small perturbations lead to self-propagating intrusions [*Stern*, 1967; *Toole and Georgi*, 1981].

Evidence for diffusive interleaving in the vicinity of the New England shelf-slope front was reported by *Voorhis et al.* [1976]. On the basis of CTD casts made while tracking neutrally buoyant floats, they estimated horizontal scales of the intrusions to be of order 10–30 km and layer thicknesses ranging from 1 to 30 m, with a typical layer thickness of about 10 m. *Ruddick and Turner* [1979] showed that these vertical scales agree with predictions based on energetics arguments, which imply a vertical scale of approximately 6 m with an uncertainty factor of 2 based on laboratory experiments. *Horne* [1978] also reported interleaving along the shelf-slope front off Nova Scotia, for which he estimated typical vertical and cross-front scales of order 10 m and 3–5 km, respectively. (As noted by *Ruddick and Turner* [1979], the observations by Horne may have been dominated by diffusive fluxes rather than double-diffusive fluxes. Hence the vertical scales may have been set by a different process than those observed by *Voorhis et al.*, [1976].)

An example of interleaving from the final survey of the 1996 rhodamine dye study is shown in Plate 3. The alternating horizontal bands of relatively high and low temperature and salinity anomalies are readily apparent and indicate a typical vertical scale of 5–10 m consistent with observations of previous investigators.

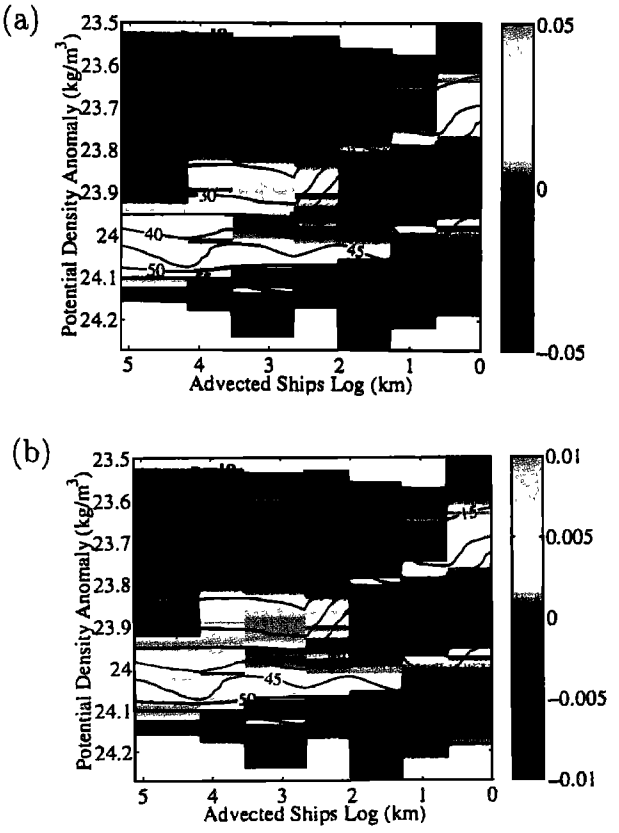

Plate 3. (a) Temperature and (b) salinity anomalies along isopycnal surfaces from a meridional transect taken during survey 3 of the 1996 rhodamine dye study. Anomalies along isopycnals were computed by subtracting the mean value for that isopycnal as computed over the length of the transect. Contour lines of pressure are plotted in each panel.

Laboratory studies of *Ruddick and Turner* [1979] suggested that the horizontal propagation speed of double-diffusive intrusions scales approximately as

$$u \approx \frac{1}{200} N H, \tag{23}$$

where N is the buoyancy frequency and H is the vertical wavelength of the intrusions (this result was first published by *Ruddick and Hebert* [1988]). From this result, using a typical buoyancy frequency for the CMO site of $N = 0.02$ rad s^{-1} (10 cph) and a vertical wavelength of $H = 10$ m, the inferred propagation speed of the observed intrusions is $u \approx 1 \times 10^{-3}$ m s^{-1}, which is too small to be resolved by shipboard ADCP observations. However, using this velocity scale and an appropriate timescale, an effective horizontal dispersion due to interleaving, $\kappa_h \approx u^2 T$, can be estimated. Assuming as a timescale the time it would take an anomaly to diffuse away because of vertical diffusion (i.e., the effective lifetime of an anomaly), $T \approx H^2/\kappa_z$, the horizontal dispersion becomes

$$\kappa_h \approx u^2 T = \frac{u^2 H^2}{\kappa_z} = \frac{1}{200^2} \frac{N H^4}{\kappa_z}. \tag{24}$$

This approach is similar to that used by *Joyce* [1977] where the effective horizontal diffusivity due to lateral intrusions is assumed to be in statistical equilibrium with the vertical diffusivity.

For a vertical wavelength of $H = 10$ m and a vertical diffusivity of $\kappa_z = 10^{-5}$ m^2 s^{-1}, consistent with the dye, the above scaling gives a timescale of $T \approx 100$ days and a corresponding effective horizontal diffusivity of $\kappa_h \approx 10$ m^2 s^{-1} (Table 5). While this horizontal diffusivity is certainly enticing as an explanation for the observed dispersion in the CMO dye studies, the timescale associated with this process is much too long to be relevant to the 2.5–5 day experiments described in sections 2 and 3. On the other hand, assuming a smaller vertical scale of $H = 1$ m so that the timescale $T \approx 1$ day is of the same order as the dye experiments, the effective horizontal diffusivity $\kappa_h \approx 10^{-3}$ m^2 s^{-1} becomes much smaller than that observed from the dye studies. Similar estimates for an intermediate value of $H = 3$ m are given in Table 5 and again show that the contribution to the effective horizontal diffusivity would be too small to explain the observed dispersion.

Table 5. Estimated Propagation Speeds, Timescales, and Effective Horizontal Diffusivities for Various Values of the Vertical Scale of the Intrusions[a]

	$H = 1$ m	$H = 3$ m	$H = 10$ m
u, m s^{-1}	10^{-4}	3×10^{-4}	10^{-3}
T, days	1	10	100
κ_h, m^2 s^{-1}	10^{-3}	0.1	10

[a]Here κ_z is assumed to be of order 10^{-5} m^2 s^{-1}.

The above analysis thus implies that lateral intrusions also cannot explain the dispersion observed during the CMO dye studies. In other words the missing diffusivities $\kappa_{\text{missing}} \approx 0.2$–$4.6$ m^2 s^{-1} obtained in section 4 are still unaccounted for.

6. Discussion

In sections 4 and 5, two existing paradigms of lateral dispersion were examined in an attempt to explain the lateral dispersion observed during the CMO dye experiments. The first was vertical shear dispersion, and the second was dispersion by interleaving water masses. It was shown that a significant part of the irreversible lateral dispersion observed during the CMO dye studies could not be accounted for by these mechanisms, and that some other mechanism was required to account for horizontal diffusivities of $\kappa_{\text{missing}} \approx 2.9$–$4.6$ m^2 s^{-1} for 1995 and 1996 rhodamine dye studies and $\kappa_{\text{missing}} \approx 0.2$–$0.4$ m^2 s^{-1} for the 1996 fluorescein and the 1997 rhodamine dye studies. We now speculate briefly on an alternative mechanism that we believe may explain the observed diffusion, namely, dispersion by vortical motions caused by the relaxation of diapycnal mixing events. This mechanism is described in some detail by *Sundermeyer* [1998], and is the subject of ongoing investigation. It will therefore be only briefly discussed here.

The proposed mechanism relies on the fact that vertical mixing in the ocean is not uniform in space and time. Rather, it is episodic, consisting of isolated events that are the result of breaking internal waves (Figure 6) [e.g., *Phillips*, 1966; *Garrett and Munk*, 1972]. The result of episodic mixing is that localized regions of low stratification are generated preferentially in regions of high mixing. These low-stratification regions result in local horizontal pressure gradients that cause the well-mixed fluid to adjust laterally, forming "blini" or pancakes [*Phillips*, 1966]. The process of adjustment may lead to two types of motions, a slumping velocity that is directed radially outward and, in the case of geostrophic adjustment, an azimuthal velocity that is geostrophically balanced. For both types of motions the net effect of the adjustment is the same; the dye will be displaced laterally.

For a single event the lateral displacement of the dye is appropriately described as an advective process. However, for a large number of events the sum of the displacements can be thought of as a random walk with rms step size equal to the rms horizontal displacement averaged over the events, i.e., an effective lateral diffusivity.

As shown by *Sundermeyer* [1998], scale analysis applied to the horizontal momentum balance implies that for a series of mixing events and a given vertical diffusivity, there exists an optimal scale of mixing events for which a maximum effective horizontal diffusivity results. This maximum diffusivity is predicted to occur

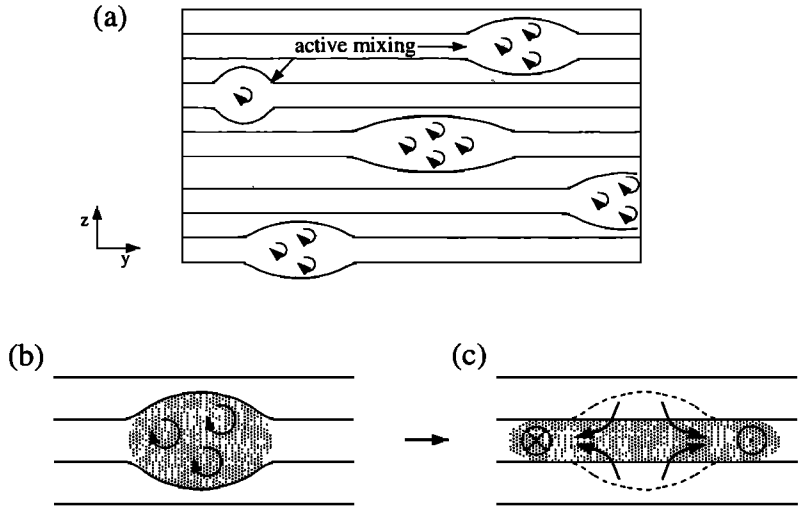

Figure 6. (a) Schematic of proposed mechanism of lateral dispersion showing diapycnal mixing that is episodic in space and time. (b) A single mixing event. (c) The ensuing lateral spreading as the stratification adjusts back to its original level.

for events of horizontal scales comparable to the internal deformation radius and vertical scales large enough that events adjust geostrophically. For the CMO dye experiments the predicted horizontal diffusivity due to the relaxation of mixing events scales as

$$\kappa_H \approx \left(\frac{3}{2}\right)\left(\frac{N^2}{f^2}\right)\left(\frac{R^2}{L^2}\right)\kappa_z, \tag{25}$$

where N is the local buoyancy frequency, f is the Coriolis parameter, $R = \frac{\Delta N h}{f}$ is the radius of deformation associated with the mixing events, ΔN is the change in stratification associated the density anomaly, L is their horizontal scale, and κ_z is the background vertical diffusivity. For values appropriate to the CMO dye studies, i.e., $N^2/f^2 \approx (0.1 \text{ to } 1.1) \times 10^5$ and $R^2/L^2 \approx 1$, the resulting lateral diffusivities due to this mechanism are of order $\kappa_H \approx 0.1\text{–}1.1 \text{ m}^2 \text{ s}^{-1}$.

The above estimates of dispersion by vortical motions are roughly consistent with the observed horizontal diffusivities for the 1996 fluorescein and 1997 rhodamine dye experiments, $\kappa_{\text{irrev}} = 0.5$ and $0.3 \text{ m}^2 \text{ s}^{-1}$, respectively. However, they are still somewhat small compared to the dispersion observed during the 1995 and 1996 rhodamine dye experiments, $\kappa_{\text{irrev}} = 4.9$ and $4.6 \text{ m}^2 \text{ s}^{-1}$, respectively. Indeed, it could be argued that these estimates are scarcely larger than the predictions of section 4 for shear dispersion. However, the vortical motion estimates are based on scaling results alone and are not an exact prediction. Also, as discussed by *Sundermeyer* [1998], these estimates may represent lower bounds on the dispersion by this mechanism.

7. Conclusions

Lateral dispersion over the New England continental shelf was examined using dye studies conducted during the Coastal Mixing and Optics experiment. Reversible and irreversible components of the lateral dispersion of the dye were defined using a simple model of vertical shear and horizontal strain. Total diffusivities (reversible plus irreversible) estimated from the vertical integral of tracer ranged from $\kappa_\zeta = 2.5$ to $12.7 \text{ m}^2 \text{ s}^{-1}$. Irreversible diffusivities estimated from the dye along the target density surface were somewhat smaller and ranged from $\kappa_{\text{irrev}} = 0.3$ to $4.9 \text{ m}^2 \text{ s}^{-1}$. For both the total dispersion and the irreversible dispersion concomitant estimates of the larger-scale horizontal strain at scales of 1–10 km ranged from $\gamma = 1.9 \times 10^{-6}$ to $4.0 \times 10^{-6} \text{ s}^{-1}$.

By using the field data from the CMO dye studies, the role of vertical shear dispersion as a mechanism of lateral dispersion was examined through a linear shear dispersion model. Upper bound estimates of the vertical diffusivities inferred from the dye and of the initial horizontal and vertical patch variances were used to obtain upper bound estimates of the effective lateral dispersion due to shear dispersion. The model predicted that on timescales of 2.5–5.0 days, mean and oscillatory shear dispersion over the continental shelf were generally comparable in magnitude. Most importantly, however, this analysis showed that shear dispersion alone cannot account for the irreversible diffusivities observed during the CMO dye studies. Upper bound predictions for shear dispersion accounted for between 1 and 50% of the observed lateral dispersion; that is, in some cases the shear dispersion predictions were more than an order of magnitude smaller than the observed dispersion. The inclusion of a time-dependent vertical diffusivity, as well as the use of level versus layer shears in this model, further strengthened this result. This suggests that some other mechanism is required to contribute additional horizontal diffusivities

of $\kappa_{missing} \approx 2.9$–$4.6\ m^2\ s^{-1}$ for the 1995 and 1996 rhodamine dye studies and $\kappa_{missing} \approx 0.2$–$0.4\ m^2\ s^{-1}$ for the 1996 fluorescein and the 1997 rhodamine dye studies.

A second mechanism examined as a possible explanation for the observed horizontal dispersion was mixing due to lateral intrusions. Two types of intrusions were considered: large-scale water mass intrusions and diffusive interleaving. In the case of large-scale intrusions the vertical scales of the intrusions were comparable to the vertical scales of the dye patches so that the effect of the intrusions on the dye patches was more likely advective rather than diffusive. In the case of diffusive interleaving, scaling arguments showed that intrusions with vertical scales of order $H \approx 10$ m would have had diffusive timescales that were much too long to affect the 2.5–5 day dye studies. Alternatively, intrusions with vertical scales of order a few meters would also have been ineffective because the resulting diffusivities would have been too small.

In light of these results, dispersion by vortical motions caused by the relaxation of diapycnal mixing events was suggested as an alternative mechanism of lateral dispersion. As shown by *Sundermeyer* [1998], simple scaling arguments applied to the horizontal momentum equations suggest that in at least two of the four experiments this mechanism could account for the observed dispersion. Whether the remaining discrepancy is due to the predicted diffusivities being a lower bound or whether there is yet another mechanism of lateral dispersion at work remains to be seen and is the subject of ongoing investigation.

Acknowledgments. This work was funded by the Office of Naval Research under grant N00014-95-1-0633 and through AASERT fellowship N00014-95-1-1063. The authors thank Tim Duda, Harvey Seim, Chris Rehmann, Neil Oakey, and Blair Greenan for insightful discussions. Also, thanks to Terry Donoghue, Cindy Sellers, Stew Sutherland, Craig Marquette, Brian Connolly, Brian Guest, Scott Madin, Dave Ciochetto, and the crew of the R/V *Oceanus* for invaluable assistance with the CMO dye studies. Processing of the raw shipboard ADCP data was done by Harvey Seim. Initial processing of the dye data was done by Stew Sutherland and Cindy Sellers. This is WHOI contribution 10209.

References

Batchelor, G. K., The application of the similarity theory of turbulence to atmospheric diffusion, *Q. J. R. Meteorol. Soc.*, *76*, 133–146, 1950.

Bowden, K. F., Horizontal mixing in the sea due to a shearing current, *J. Fluid Mech.*, *21*, 83–95, 1965.

Chatwin, P. C., On the longitudinal dispersion of passive contaminant in oscillatory flows in tubes, *J. Fluid Mech.*, *71*, 513–527, 1975.

Csanady, G. T., Accelerated diffusion in the skewed shear flow of lake currents, *J. Geophys. Res.*, *71*, 411–420, 1966.

Elder, J. W., The dispersion of marked fluid in turbulent shear flow, *J. Fluid Mech.*, *5*, 544–560, 1959.

Garrett, C., and W. Munk, Oceanic mixing by breaking internal waves, *Deep Sea Res. Oceanogr. Abstr.*, *19*, 823–832, 1972.

Geyer, W. R., and J. R. Ledwell, Massachusetts Bay dye study, *Final Report*, 13 pp., Mass. Water Resour. Auth., Charlestown, Mass., 1994.

Geyer, W. R., and J. R. Ledwell, Boundary mixing in Massachusetts Bay, *Report ENQUAD 1997-09*, 20 pp., Mass. Water Resour. Auth., Charlestown, Mass., 1997.

Horne, E. P. W., Interleaving at the subsurface front in the slope water off Nova Scotia, *J. Geophys. Res.*, *83*, 3659–3671, 1978.

Houghton, R. W., Lagrangian flow at the foot of a shelfbreak front using a dye tracer injected into the bottom boundary layer, *Geophys. Res. Lett.*, *24*, 2035–2038, 1997.

Journel, A. G., and C. J. Huijbregts, *Mining Geostatistics*, 600 pp., Academic, San Diego, Calif., 1978.

Joyce, T. M., A note on the lateral mixing of water masses, *J. Phys. Oceanogr.*, *7*, 626–629, 1977.

Kolmogorov, A. N., The local structure of turbulence in incompressible viscous fluid for very large Reynolds' numbers., *Dokl. Akad. Nauk U.S.S.R.*, *30*, 301–305, 1941.

Kullenberg, G., Vertical diffusion in shallow waters, *Tellus*, *23*, 129–135, 1971.

Ledwell, J. R., A. J. Watson,, and C. S. Law, Mixing of a tracer released in the pycnocline, *J. Geophys. Res.*, *103*, 21,499–21,529, 1998.

Okubo, A., Oceanic diffusion diagrams, *Deep Sea Res. Oceanogr. Abstr.*, *18*, 789–802, 1971.

Phillips, O. M., *Dynamics of the Upper Ocean*, 1st ed., 261 pp., Cambridge Univ. Press, New York, 1966.

Richardson, L. F., Atmospheric diffusion shown on a distance-neighbour graph, *Proc. R. Soc., London A*, *110*, 709–737, 1926.

Richardson, L. F., and H. Stommel, Note on eddy diffusion in the sea, *J. Meteor.*, *5*, 238–240, 1948.

Ruddick, B. R., and D. Hebert, The mixing of meddy "Sharon", in *Small-Scale Turbulence and Mixing in the Ocean: Proceedings of the 19th International Liege Colloquium on Ocean Hydrodynamics*, edited by J. C. J. Nihoul and B. M. Jamart, *Elsevier Oceanogr. Ser.*, *46*, 249–261, 1988.

Ruddick, B. R., and J. S. Turner, The vertical length scale of double-diffusive intrusions, *Deep Sea Res., Part A*, *26*, 903–913, 1979.

Saffman, P. G., The effect of wind shear on horizontal spread from an instantaneous ground source, *Q. J. R. Meteorol. Soc.*, *88*, 382–393, 1962.

Smith, R., Dispersion of tracers in the deep ocean, *J. Fluid Mech.*, *123*, 131–142, 1982.

Stern, M. E., Lateral mixing of water masses, *Deep Sea Res. Oceanogr. Abstr.*, *14*, 747–753, 1967.

Stommel, H., Horizontal diffusion due to oceanic turbulence, *J. Mar. Res.*, *8*, 199–255, 1949.

Stommel, H., and K. N. Fedorov, Small scale structure in the temperature and salinity near Timor and Mindanao, *Tellus*, *19*, 306–325, 1967.

Sundermeyer, M. A., Studies of lateral dispersion in the ocean, Ph.D. thesis, 215 pp., Mass. Inst. of Technol. / Woods Hole Oceanogr. Inst. Joint Program, Woods Hole, 1998.

Taylor, G. I., Diffusion by continuous movements, *Proc. London Math. Soc. A*, *20*, 196–212, 1921.

Taylor, G. I., Dispersion of soluble matter in solvent flowing slowly through a tube, *Proc. R. Soc. London, Ser. A, 219*, 186–203, 1953.

Toole, J. M., and D. T. Georgi, On the dynamics and effects of double-diffusively driven intrusions, *Prog. Oceanogr., 10*, 123–145, 1981.

Townsend, A. A., The diffusion of heat spots in isotropic turbulence, *Proc. R. Soc. London, Ser. A, 209*, 418–430, 1951.

Vasholz, D. P., and L. J. Crawford, Dye dispersion in the seasonal thermocline, *J. Phys. Oceanogr., 15*, 695–711, 1985.

Voorhis, A. D., D. C. Webb,, and R. C. Millard, Current structure and mixing in the shelf/slope water front south of New England, *J. Geophys. Res., 81*, 3695–3708, 1976.

Wanninkhof, R., et al., Gas exchange, dispersion, and biological productivity on the west Florida shelf: Results from a Lagrangian tracer study, *Geophys. Res. Lett., 24*, 1767–1770, 1997.

Young, W. R., P. B. Rhines,, and C. J. R. Garrett, Shear-flow dispersion, internal waves and horizontal mixing in the ocean, *J. Phys. Oceanogr., 12*, 515–527, 1982.

J. R. Ledwell, Department of Applied Physics and Ocean Engineering, Mail Stop 12, Woods Hole Oceanographic Institution, Woods Hole, MA 02543. (jledwell@whoi.edu)

M. A. Sundermeyer, School of Marine Science and Technology, University of Massachusetts Dartmouth, 706 South Rodney French Boulevard, New Bedford, MA 02744. (msundermeyer@umassd.edu)

(Received April 2, 1999; revised May 30, 2000; accepted May 31, 2000.)